




MRI radiomics analysis of molecular alterations in low-grade gliomas

Ben Shofty^{1,2} · Moran Artzi^{2,3} · Dafna Ben Bashat^{2,3,5}  · Gilad Liberman⁴ · Oz Haim¹ · Alon Kashanian^{1,2} · Felix Bokstein^{2,6} · Deborah T. Blumenthal^{2,6} · Zvi Ram^{1,2} · Tal Shahar^{1,7}

Received: 12 July 2017 / Accepted: 4 December 2017 / Published online: 21 December 2017
© CARS 2017

Abstract

Purpose Low-grade gliomas (LGG) are classified into three distinct groups based on their IDH1 mutation and 1p/19q codeletion status, each of which is associated with a different clinical expression. The genomic sub-classification of LGG requires tumor sampling via neurosurgical procedures. The aim of this study was to evaluate the radiomics approach for noninvasive classification of patients with LGG and IDH mutation, based on their 1p/19q codeletion status, by testing different classifiers and assessing the contribution of the different MR contrasts.

Methods Preoperative MRI scans of 47 patients diagnosed with LGG with IDH1-mutated tumors and a genetic analysis for 1p/19q deletion status were included in this study. A total of 152 features, including size, location and texture, were extracted from fluid-attenuated inversion recovery images, T₂-weighted images (WI) and post-contrast T₁ WI. Classification was performed using 17 machine learning classifiers. Results were evaluated by a fivefold cross-validation analysis.

Results Radiomic analysis differentiated tumors with 1p/19q intact ($n = 21$; astrocytomas) from those with 1p/19q codeleted ($n = 26$; oligodendrogliomas). Best classification was obtained using the Ensemble Bagged Trees classifier, with sensitivity = 92%, specificity = 83% and accuracy = 87%, and with area under the curve = 0.87. Tumors with 1p/19q intact were larger than those with 1p/19q codeleted (46.2 ± 30.0 vs. 30.8 ± 16.8 cc, respectively; $p = 0.03$) and predominantly located to the left insula ($p = 0.04$).

Conclusion The proposed method yielded good discrimination between LGG with and without 1p/19q codeletion. Results from this study demonstrate the great potential of this method to aid decision-making in the clinical management of patients with LGG.

Keywords MRI · Radiomics · Low-grade gliomas · 1p/19q Codeletion · Machine learning classifiers

Ben Shofty and Moran Artzi contributed equally to this work.

✉ Dafna Ben Bashat
dafnab@tlvmc.gov.il

¹ Division of Neurosurgery, Tel Aviv Sourasky Medical Center, 6 Weizman St., 64239 Tel Aviv, Israel

² Sackler Faculty of Medicine, Tel Aviv University, Tel Aviv, Israel

³ The Functional Brain Center, Tel Aviv Sourasky Medical Center, 6 Weizman St., 64239 Tel Aviv, Israel

⁴ Department of Chemical Physics, Weizmann Institute of Science, Rehovot, Israel

⁵ Sagol School of Neuroscience, Tel Aviv University, Tel Aviv, Israel

⁶ Neuro-Oncology Service, Tel-Aviv Medical Center, Tel Aviv, Israel

Introduction

Diffuse low-grade gliomas (LGG) are grade II tumors characterized by having a variable clinical course and outcome according to the revised World Health Organization (WHO) classification [1]. Most diffuse LGG are associated with mutations in the isocitrate dehydrogenase 1 gene (IDH1). Patients with IDH1-mutated tumors typically have an indolent course and a more favorable outcome [2–4]. In contrast, wild-type IDH1 LGG tend to rapidly acquire multiple complex genetic alterations and transform to glioblastomas early in their course [4]. A distinct subtype of IDH1-mutated diffuse gliomas includes those associated with deletions in chromosome arms 1p and 19q

⁷ Department of Neurosurgery, Shaare Zedek Medical Center, Jerusalem, Israel

(1p/19q codeletion), classically recognized as oligodendrogliomas [5,6]. Patients with 1p/19q codeleted tumors respond better both to chemotherapy and to radiation and are associated with longer survival compared to patients with non-codeleted IDH1 mutated tumors [6]. The significance of the genetic alterations that occur in diffuse LGG was further emphasized in the updated brain tumor classification of the WHO [7]. Tumor types and grades that have been historically determined by histology are now defined and treated based on these genetic alterations [7].

Currently, IDH and 1p/19q status of the tumor cannot be determined without obtaining tissue samples via invasive surgical procedures. These surgeries usually involve hospitalization and may be associated with morbidity, mortality and high costs. This has spurred a tremendous interest in developing alternative methods to noninvasively classify tumors into different subtypes. Several studies have aimed to identify IDH mutation status using magnetic resonance imaging (MRI). However, very few attempts have been made to predict the codeletion status of 1p/19q. Identification of 2-hydroxyglutarate (2HG), the metabolite of mutated IDH1, by MR spectroscopy (MRS) was suggested as a biomarker for IDH1 mutation by several groups [8–10]. Despite initial promising results, the need for special quantitative analysis and a customized in vivo MRS sequence that is not routinely performed limits the usefulness of this method. Other researchers used multiparametric MRI data to predict the mutation status of IDH1, such as histogram analysis of diffusion-weighted imaging (DWI), dynamic-susceptibility contrast perfusion MRI [11], arterial spin-labeling (ASL) MRI [12], and radiomics approach [13,14]. Only a few studies investigated the use of quantitative tumor location measurement [15] as well as application of advanced classification methods [16,17] to

differentiate between LGG based on their 1p/19q codeletion.

Radiomics analysis, based on computerized tomography (CT) and MRI data, was proposed to further characterize diseases and their underlying processes beyond what can be observed by the radiologist's naked eye. Advanced image analysis can convert standard medical images into higher-dimensional quantitative data, potentially reflecting the underlying pathology [18–20]. Although radiomics can be potentially applied to a large number of clinical conditions, based on conventional imaging methods, currently the most widespread use of this approach is in cancer research [13,18–21]. Radiomics can provide a noninvasive means of improving decision-making in cancer treatment at lower cost than current invasive approaches. In this work, we aimed to apply radiomics analysis to predict the 1p/19q codeletion status in patients with IDH1-mutated diffuse LGG while testing different classifiers, and to assess the contribution of the different MR contrasts and lesion location.

Methods

Study participants

This is a retrospective analysis of data obtained from 47 patients with confirmed histological identification of grade II LGG, positive IDH1-mutated tumors, and genetic analysis for 1p/19q codeletion status. As a general practice in our institute, we recommend all patients with IDH1 mutated tumors to be tested for 1p/19q codeletion status. The study was approved by the institutional review board. Patients' characteristics are given in Table 1.

Table 1 Patient's clinical characteristics

Variable	Total	IDH Mutation with 1p/19q codeletion	IDH Mutation without 1p/19q codeletion	<i>p</i>
Number	47	26	21	
Age	37.7 ± 10.6	40.3 ± 10.8	36.7 ± 9.7	
Female/male	20/27	11/15	9/12	
Tumor location				
Frontal	53%	52%	55%	0.79
Parietal	16%	15%	17%	0.87
Temporal	30%	23%	38%	0.12
Occipital	2%	2%	2%	0.88
Limbic	48%	44%	52%	0.44
Sub-lobar	43%	33%	55%	0.03
Cerebellum	0%	0%	0%	–
Brain stem	3%	0%	7%	–

Immunohistochemistry

Immunohistochemistry for IDH1-R132H was done on 5- μ m-thick formalin-fixed, paraffin-embedded tumor sections. Antigen retrieval was performed in citrate buffer (pH 6.0) in a microwave oven. Antibody specific for the mutant IDH1-R132H protein (H09, dil 1:100; Dianova, Hamburg, Germany) was used. Secondary antibody labeled with streptavidin biotin kit (Universal) was used as a detection system (Dako, Denmark). A senior pathologist evaluated the results of the immunostaining.

Evaluation of 1p/19q codeletion status

Loss of heterozygosity (LOH) in chromosomes 1p and 19q was assessed by polymerase chain reaction (PCR)-based microsatellite analysis, detailed elsewhere [22].

Imaging protocol

Preoperative MRI scans were performed as part of the patients' clinical assessment. Data were collected from different MRI systems from different sites and vendors with various acquisition parameters, including 1.5 and 3.0 Tesla scanners: 10 scans were performed on a Philips system, 33 scans were performed on a GE system, and 4 on a Siemens system. The protocol included fluid attenuation inversion recovery (FLAIR): repetition time (TR) = 6000–10,002 ms, echo time (TE) = 85–151 ms, inversion time (IT) = 2000–2750 ms, voxel size = 0.4–4.8 cc; spin-echo (SE) T₂-weighted images (T₂WI): TR = 2500–14820 ms, TE = 84–110 ms, voxel size = 0.7–4.8 cc; post-contrast T₁ WI (T₁WIGd) spoiled gradient echo (SPGR): repetition time (TR) = 7–17 ms, echo time (TE) = 2–4 ms; voxel size = 0.4–4.8 cc or post-contrast SE T₁WI: TR = 400–536 ms, TE = SE = 7–20 ms, voxel size = 0.25–4.4 cc.

Image preprocessing

Figure 1 provides an overview of the data analysis pipeline.

MRI data preprocessing

Preprocessing included realignment of all anatomical images to the same space using FMRIB Software Library (FSL) linear image registration tool and affine transformation (12 parameters model), [23] as well as skull stripping using the FSL brain extraction tool [24]. To overcome heterogeneity in image intensity caused by the use of different scanners and acquisition parameters, the intensity of all anatomical images (FLAIR, T₁WIGd and T₂WI) was normalized relative to the mean value of the normal-appearing white matter (NAWM) area. The NAWM was extracted from the anatomical images

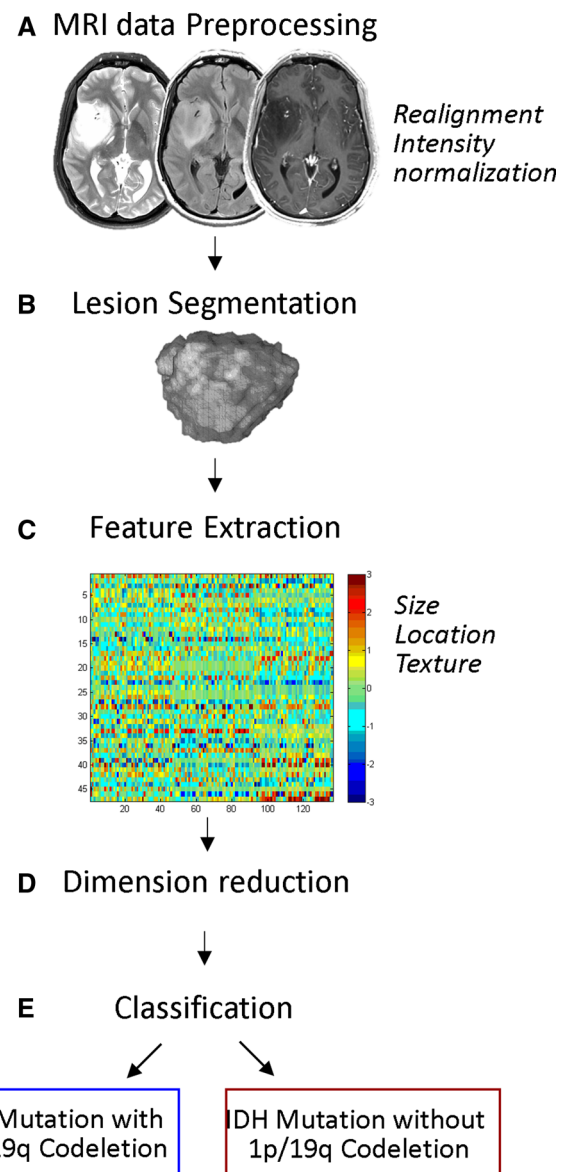


Fig. 1 Analysis pipeline

using FSL's automatic segmentation tool (FAST), incorporating the hidden Markov random field (HMRF) model and an associated expectation-maximization algorithm [25] after removal of the predefined lesion areas. The obtained mask was eroded to minimize partial volume effect and later used as a reference area for intensity normalization.

Lesion segmentation

The lesion area was defined as the abnormal hyperintensity area on T₂WI/FLAIR images. Segmentation of the lesion area was performed using AnalyzeDirect software (version 11.0, Mayo Clinic, Rochester, MN, USA). In each patient, three regions of interest (ROIs) were selected as the middle

slice (ROI1), middle slice + 1 (ROI2) and middle slice-1 (ROI3), ranked as the slice with minimum, median and maximum value, in order to account for tumor heterogeneity and to increase the amount of available data.

Feature extraction

A total of 152 size, location and textural features were extracted from the lesion area of each patient using Matlab 2017a (The MathWorks Inc., Natick, MA): Size and location features included lesion volume (measured for the entire lesion area) and location calculated by partitioning the brain into 16 locations: left and right, frontal, parietal, temporal, occipital, limbic sub-lobar lobes, cerebellum and brainstem based on the Talairach space anatomy template (total of 17 features). First-order statistical features included mean, median, 25th and 75th percentiles, standard deviation, maximum, minimum, variance, kurtosis, skewness. Second-order statistical features included contrast, correlation, energy, entropy and homogeneity [26]. Each of the textural features was calculated for the ROIs of the lesions and for the three MRI contrasts (FLAIR, T₁WIGd and T₂WI, total of 152 features).

Dimension reduction

Dimension reduction was performed on the 152 features in order to improve classification. Initially, all features were standardized before classification as follows:

$$X_{SDi} = \frac{[X_i - \bar{X}]}{\sigma_{\bar{X}}}$$

where x_i is the value of individual subject for given feature and \bar{X} and $\sigma_{\bar{X}}$ are mean and standard deviation values of the entire group for a given parameter.

The one-sample Kolmogorov–Smirnov test was used to test the distribution of each feature. Significant differences ($p < 0.05$) between groups (tumoral versus non-tumoral components) were tested using the Mann–Whitney U test/ t test (depending on data distribution). Next, principal component analysis (PCA) was applied only on features that were significantly different ($p < 0.05$) between groups.

Classification

Classification of the LGG tumors based on the MRI images was performed using the Matlab classification learner tool. The classification performances were tested by 17 machine learning algorithms including by support vector machine (SVM), k -nearest neighbor (k NN), and Ensemble classifiers: (1) linear SVM, (2) quadratic SVM, (3) cubic SVM, (4) fine Gaussian SVM (kernel scale set to square root of the num-

ber of features (F)/4), (5) medium Gaussian SVM (kernel scale set to square root (F)), (6) coarse Gaussian SVM kernel scale set to square root (F)*4, (7) fine k NN (with the number of neighbors set to 1), (8) coarse k NN (with the number of neighbors set to 100), (9) medium k NN, (10) cosine k NN, (11) cubic k NN, (12) weighted k NN (with the number of neighbors set to 10 for [9–12]), (13) Boosted Trees, (14) Subspace Discriminant, (15) Subspace k NN and (16) RUSBoosted Trees.

Evaluation

The results were evaluated using a fivefold cross-validation scheme of randomly splitting the data into training and testing sets. Sensitivity, specificity, accuracy and receiver operating characteristics (ROC) of the classification results were calculated for each tested condition.

Results

Differences between groups

Radiomic analysis significantly ($p < 0.05$) differentiated tumors with 1p/19q intact ($n = 21$; astrocytomas) from those with 1p/19q codeleted ($n = 26$; oligodendrogliomas) by 39/152 imaging features (Table 2). Figure 2 demonstrates the different radiomics signatures for each group. For location features, as expected, the majority of tumors in both groups were detected in the cerebrum. However, there was a significant difference ($p = 0.041$) for the left sub-lobar lobe, with a larger incidence being detected for the patients without 1p/19q codeletion (52%) in comparison with patients with a 1p/19q codeletion (23%). Figure 3a illustrates the distribution of lesion location across the groups. Thirty nine textural features showed significant group differences ($p < 0.05$), with the majority of differences detected for the T₂WI (19 features) and for the T₁WIGd (15 features), and only a few for the FLAIR images (4 features) (Fig. 2; Table 2). No significant age or gender differences were detected between groups. Following the PCA, 9 components were found to explain 95% of the variance, and were subsequently used for classification.

Classification results

Seventeen machine learning algorithms were tested based on the nine principal components, and their sensitivity, specificity and accuracy are presented in Table 3. The best classification results were obtained using the Ensemble Bagged Trees classifier with a sensitivity of 92%, a specificity of 83% and an accuracy of 87%, and with an area under the

Table 2 Features that showed significant group differences

Image contrast	Feature	<i>p</i>
	Left sub-lobar	0.041
FLAIR	Minimum ^{min}	0.047
FLAIR	Entropy ^{max}	0.047
FLAIR	STD ^{min}	0.033
FLAIR	Variance ^{min}	0.033
T ₁ WI + Gd	Max ^{min}	0.021
T ₁ WI + Gd	Mean ^{min,med}	0.020, 0.017
T ₁ WI + Gd	Median ^{min,med}	0.016, 0.016
T ₁ WI + Gd	Prctile ²⁵ ^{min,med}	0.020, 0.021
T ₁ WI + Gd	Prctile ⁷⁵ ^{min,med}	0.016, 0.013
T ₁ WI + Gd	Entropy ^{mid}	0.047
T ₁ WI + Gd	Energy ^{max}	0.029
T ₁ WI + Gd	Kurtosis ^{med,max}	0.016, 0.039
T ₁ WI + Gd	Skewness ^{max,med}	0.002, 0.014
T ₂ WI	Mean ^{min,med,max}	0.003, 0.004, 0.001
T ₂ WI	Median ^{min,med,max}	0.003, 0.003, 0.001
T ₂ WI	Max ^{min,med,max}	0.0001, 0.020, 0.031
T ₂ WI	Min ^{med,max,min}	0.00003, 0.028, 0.048
T ₂ WI	Prctile ²⁵ ^{min,med,max}	0.001, 0.001, 0.001
T ₂ WI	Prctile ⁷⁵ ^{min,med,max}	0.005, 0.002, 0.003
T ₂ WI	Skewness ^{min}	0.009

Slice ranked (*min* minimum, *med* median, *max* maximum)

curve (AUC) of the ROC curve for 1p/19q codeletion prediction of 0.87 (Fig. 3b).

Discussion

In this study, we applied radiomics analysis to MRI data for noninvasive detection of 1p/19q codeletion in patients with LGG. Various machine learning classifiers were tested, with the Ensemble Bagged Trees classifier achieving the best performance, with an 87.0% accuracy for the detection of 1p/19q codeletion. The classifier was trained on MRI data, which was acquired as part of routine preoperative MRI scans of patients with LGG, and can be used without the need for special imaging sequences.

1p/19q codeletion is an important genetic marker of LGG since it determines the subtype (oligodendroglioma) and the derived prognosis and treatment. Patients with 1p/19q-codeleted tumors have a better response to radiation and chemotherapy and a longer progression-free and overall survival [1,5]. Given that follow-up without intervention may be a valid therapeutic option in 1p/19q-deleted tumors, noninvasive identification of this mutation may be very beneficial for these patients, potentially sparing them unnecessary intervention.

Radiomics is a rapidly evolving technique in medical image analysis. It refers to the conversion of imaging data

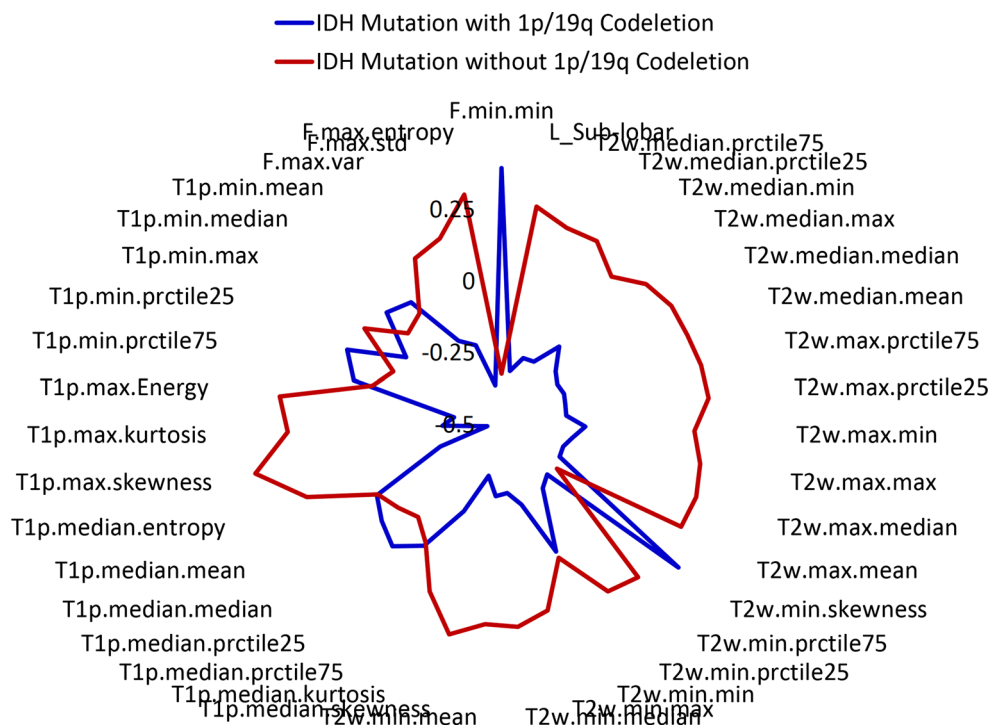
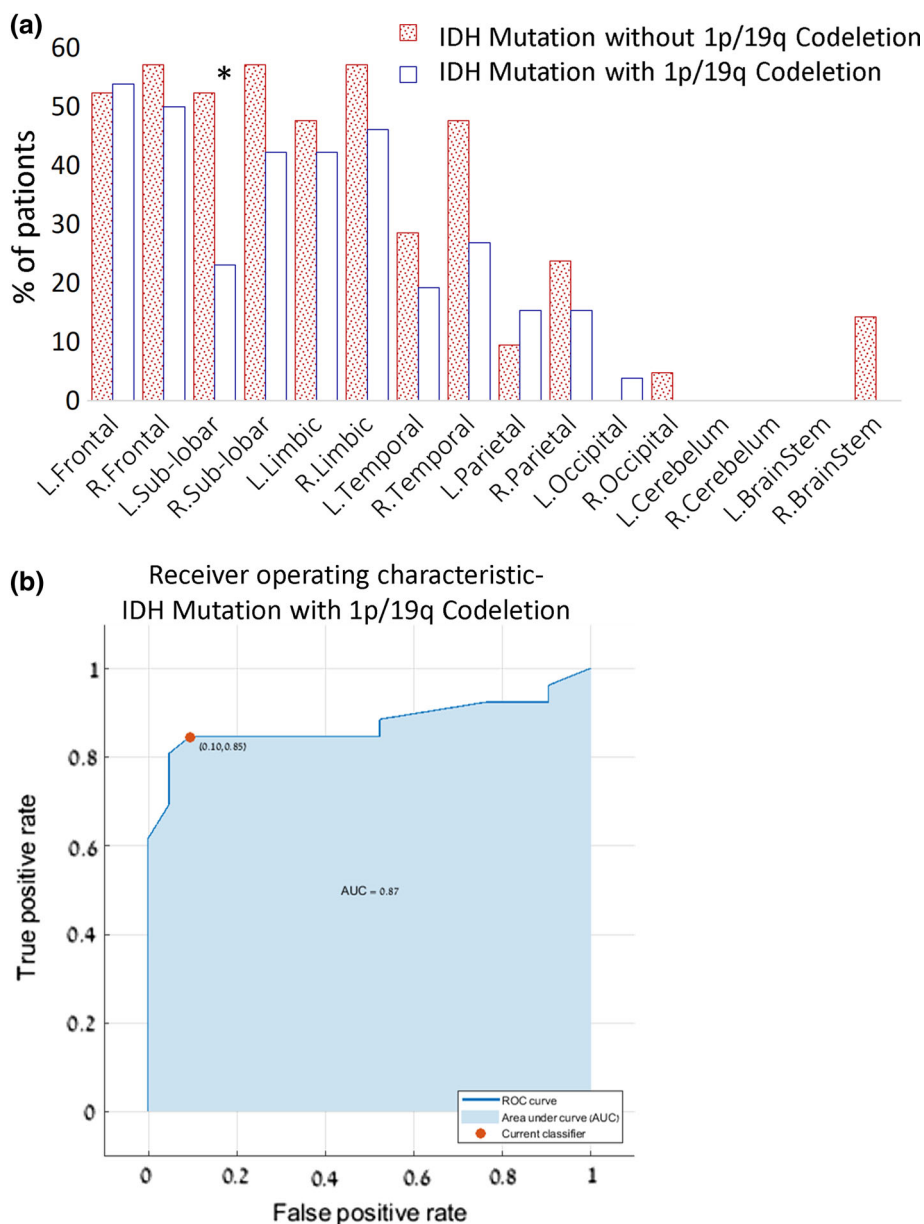


Fig. 2 Surface chart of all 34 features significantly differentiating between groups by demonstrating the unique radiomics signature obtained for each group. T1p, T₁-weighted image post-contrast agent injection; T₂W, T₂-weighted image; F, fluid attenuation inversion recovery

Fig. 3 **a** Distribution of lesion location across groups. (* = $p < 0.05$). **b** Receiver operating characteristic (ROC) curve: IDH Mutation with 1p/19q Codeletion



into a high-dimensional mineable feature space, using a large number of automatically extracted data-characterization features [18,19]. Radiomics analysis was recently used for noninvasive detection of tumor phenotypes in patients with lung and head and neck cancer, [18] to predict IDH mutation [14], and to identify molecular characteristics in high-grade gliomas [14,27]. It was recently used in LGG to predict IDH mutation status [13] and 1p/19q codeletion [17]. Promising results from these studies serve to motivate further development of radiomics in brain tumors since preoperative identification of tumor type may alter the management of these complex tumors. Results from our study support the use of a radiomics approach for 1p/19q codeletion status assessment.

Despite the increasing use of the radiomics approach for various clinical applications, this technique is not sufficiently established to be used routinely in clinical settings. This is partly due to the sensitivity of this analysis to variations in MR acquisition parameters. In the current study, we used retrospective data obtained from various MRI scanners and a large variability of parameters. Despite the considerable heterogeneity of our data, we achieved a good level of accuracy and AUC of the ROC curve values for the prediction of 1p/19q codeletions, demonstrating the robustness of the method and its potential clinical transferability for diagnostic classification of molecular alteration in LGG. However, higher sensitivity, specificity and accuracy are needed in the setting of personalized medicine and for making safe treat-

Table 3 Sensitivity, specificity and accuracy of the different classifier types

Classifier type	Specificity (%)	Sensitivity (%)	Accuracy (%)	ROC AUC
<i>Support vector machines (SVM)</i>				
Linear SVM	80	81	81	0.88
Quadratic SVM	79	79	79	0.84
Cubic SVM	75	78	77	0.84
Fine Gaussian SVM	0	55	55	0.62
Medium Gaussian SVM	75	87	81	0.85
Coarse Gaussian SVM	50	56	55	0.89
<i>Nearest neighbor classifiers (kNN)</i>				
Fine kNN	67	69	68	0.67
Medium kNN	86	63	66	0.85
Coarse kNN	0	55	55	0.47
Cosine kNN	84	83	83	0.88
Cubic kNN	71	60	62	0.86
Weighted kNN	89	66	70	0.87
<i>Ensemble classifiers</i>				
Boosted Trees	0	55	55	1.00
Bagged Trees	83	92	87	0.87
Subspace discriminant	83	79	80	0.89
Subspace kNN	68	71	70	0.83
RUSBoosted Trees	75	66	68	0.67

Sensitivity, specificity and accuracy are given in percentages. Bold indicates chosen classifier
AUC area under curve, *ROC* receiver operating characteristic

ment decisions. Thus, further studies in a prospective manner with larger cohorts are necessary to improve and confirm our results.

In this study, we extracted location and first- and second-order statistical features [26]. Texture features enabled the description of the variations in the surface intensity or patterns at the lesion area, including some that are indiscernible to the human eye [28]. Notably, texture features had previously been used for brain tumor characterization and classification [14,28,29], demonstrating the promising potential of this automated pattern recognition approach to provide objective information and to support clinical decision-making. The features that mostly contributed to the classification were T1WIGd and T2WI, which are features that reflected differences in tumor heterogeneity. This emphasizes the importance of using the radiomics features that relate to the texture of the tumors. Dimension reduction was performed on the 152 features using PCA that had been performed only on features that were significantly different between groups, in order to improve classification, to reduce over-fitting error, and to be less impacted by noise or random error [28].

Tumor location has traditionally been considered as one of the most important parameters and one that correlates with lesion growth pattern and prognosis in LGG [30]. The contribution of information on tumor location in differenti-

ating between molecular genetic subsets has been tested in a few recent studies. One study found that tumors with 1p/19q codeletion occur most frequently in the frontal lobes and have a tendency for widespread growth across the midline [31]. Two other studies concluded that quantitative tumor locations are important features and that they should be included in radiomics analysis to identify IDH mutation in LGG [13]. In line with previous publications [13,31], the majority of tumors in the current study were detected in the cerebrum. The location features were defined by dividing the brain into 16 regions based on the Talairach space anatomy template. This reconstructed template enables automatic localization of the lesion areas into well-defined regions similar to those used in traditional radiology, and thus may be superior both to manual labeling of lesion location—which may have high intra-observer variability—and to the use of available templates, such as the automated anatomical labeling atlas, which is limited to gray matter areas. In our study, location features differed significantly between the groups, but they did not contribute much to the classification results. Future studies with larger numbers of patients are needed for thorough examination of the contribution of location characteristics to classifying cranial lesions.

In conclusion, the current study demonstrates the use of radiomics analysis to identify 1p/19q codeletion status in patients with LGG based on conventional MRI. The proposed

noninvasive method may aid the treating neuro-oncologist in more accurately predicting prognosis prior to tissue diagnosis and in personalizing the follow-up and treatment regimen without the need for or prior to invasive tissue sampling. This method is also easily translatable to other tumor types and potentially to other imaging modalities.

Acknowledgements To Esther Eshkol for editorial assistance.

Compliance with ethical standards

Conflict of interest The authors declare that they have no conflict of interest.

Ethical approval All procedures performed in this study were in accordance with the ethical standards of the institutional and/or national research committee and with the 1964 Declaration of Helsinki and its later amendments or comparable ethical standards. For this type of study, formal consent was not required.

References

- Cancer Genome Atlas Research N, Brat DJ, Verhaak RG, Aldape KD, Yung WK, Salama SR, Cooper LA, Rheinbay E, Miller CR, Vitucci M, Morozova O, Robertson AG, Noushmehr H, Laird PW, Cherniack AD, Akbani R, Huse JT, Ciriello G, Poisson LM, Barnholtz-Sloan JS, Berger MS, Brennan C, Colen RR, Colman H, Flanders AE, Giannini C, Grifford M, Iavarone A, Jain R, Joseph I, Kim J, Kasaian K, Mikkelsen T, Murray BA, O'Neill BP, Pachter L, Parsons DW, Sougnez C, Sulman EP, Vandenberg SR, Van Meir EG, von Deimling A, Zhang H, Crain D, Lau K, Mallery D, Morris S, Paulauskis J, Penny R, Shelton T, Sherman M, Yena P, Black A, Bowen J, Dicostanzo K, Gastier-Foster J, Leraas KM, Lichtenberg TM, Pierson CR, Ramirez NC, Taylor C, Weaver S, Wise L, Zmuda E, Davidsen T, Demchok JA, Eley G, Ferguson ML, Hutter CM, Mills Shaw KR, Ozenberger BA, Sheth M, Sofia HJ, Tarnuzzer R, Wang Z, Yang L, Zenklusen JC, Ayala B, Baboud J, Chudamani S, Jensen MA, Liu J, Pihl T, Raman R, Wan Y, Wu Y, Ally A, Auman JT, Balasundaram M, Balu S, Baylin SB, Beroukhim R, Bootwalla MS, Bowlby R, Bristow CA, Brooks D, Butterfield Y, Carlsen R, Carter S, Chin L, Chu A, Chuah E, Cibulskis K, Clarke A, Coetzee SG, Dhalla N, Fennell T, Fisher S, Gabriel S, Getz G, Gibbs R, Guin R, Hadjipanayis A, Hayes DN, Hinoue T, Hoadley K, Holt RA, Hoyle AP, Jefferys SR, Jones S, Jones CD, Kucherlapati R, Lai PH, Lander E, Lee S, Lichtenstein L, Ma Y, Maglinte DT, Mahadeshwar HS, Marra MA, Mayo M, Meng S, Meyerson ML, Mieczkowski PA, Moore RA, Mose LE, Mungall AJ, Pantazi A, Parfenov M, Park PJ, Parker JS, Perou CM, Protopopov A, Ren X, Roach J, Sabedot TS, Schein J, Schumacher SE, Seidman JG, Seth S, Shen H, Simons JV, Sipahimalani P, Soloway MG, Song X, Sun H, Tabak B, Tam A, Tan D, Tang J, Thiessen N, Triche T Jr, Van Den Berg DJ, Veluvolu U, Waring S, Weisenberger DJ, Wilkerson MD, Wong T, Wu J, Xi L, Xu AW, Yang L, Zack TI, Zhang J, Aksoy BA, Arachchi H, Benz C, Bernard B, Carlin D, Cho J, DiCara D, Frazer S, Fuller GN, Gao J, Gehlenborg N, Haussler D, Heiman DI, Iype L, Jacobsen A, Ju Z, Katzman S, Kim H, Knijnenburg T, Kreisberg RB, Lawrence MS, Lee W, Leinonen K, Lin P, Ling S, Liu W, Liu Y, Liu Y, Lu Y, Mills G, Ng S, Noble MS, Paull E, Rao A, Reynolds S, Saksena G, Sanborn Z, Sander C, Schultz N, Senbabaoglu Y, Shen R, Shmulevich I, Sinha R, Stuart J, Sumer SO, Sun Y, Tasman N, Taylor BS, Voet D, Weinhold N, Weinstein JN, Yang D, Yoshihara K, Zheng S, Zhang W, Zou L, Abel T, Sadeghi S, Cohen ML, Eschbacher J, Hattab EM, Raghunathan A, Schniederjan MJ, Aziz D, Barnett G, Barrett W, Bigner DD, Boice L, Brewer C, Calatuzzolo C, Campos B, Carlotti CG Jr, Chan TA, Cuppini L, Curley E, Cuzzubbo S, Devine K, DiMeco F, Duell R, Elder JB, Fehrenbach A, Finocchiaro G, Friedman W, Fulop J, Gardner J, Hermes B, Herold-Mende C, Jungk C, Kendler A, Lehman NL, Lipp E, Liu O, Mandt R, McGraw M, McLendon R, McPherson C, Neder L, Nguyen P, Noss A, Nunziata R, Ostrom QT, Palmer C, Perin A, Pollo B, Potapov A, Potapova O, Rathmell WK, Rotin D, Scarpace L, Schilero C, Senecal K, Shimmel K, Shurkhay V, Sifri S, Singh R, Sloan AE, Smolenski K, Staugaitis SM, Steele R, Thorne L, Tirapelli DP, Unterberg A, Vallurupalli M, Wang Y, Warnick R, Williams F, Wolinsky Y, Bell S, Rosenberg M, Stewart C, Huang F, Grimsby JL, Radenbaugh AJ, Zhang J (2015) Comprehensive, integrative genomic analysis of diffuse lower-grade gliomas. *N Engl J Med* 372(26):2481–2498
- Parsons DW, Jones S, Zhang X, Lin JC, Leary RJ, Angenendt P, Mankoo P, Carter H, Siu IM, Gallia GL, Olivi A, McLendon R, Rasheed BA, Keir S, Nikolskaya T, Nikolsky Y, Busam DA, Tekleab H, Diaz LA Jr, Hartigan J, Smith DR, Strausberg RL, Marie SK, Shinjo SM, Yan H, Riggins GJ, Bigner DD, Karchin R, Papadopoulos N, Parmigiani G, Vogelstein B, Velculescu VE, Kinzler KW (2008) An integrated genomic analysis of human glioblastoma multiforme. *Science* 321(5897):1807–1812
- Yan H, Parsons DW, Jin G, McLendon R, Rasheed BA, Yuan W, Kos I, Batinic-Haberle I, Jones S, Riggins GJ, Friedman H, Friedman A, Reardon D, Herndon J, Kinzler KW, Velculescu VE, Vogelstein B, Bigner DD (2009) IDH1 and IDH2 mutations in gliomas. *N Engl J Med* 360(8):765–773
- Cohen AL, Holmen SL, Colman H (2013) IDH1 and IDH2 mutations in gliomas. *Curr Neurol Neurosci Rep* 13(5):345
- Boots-Sprenger SH, Sijben A, Rijntjes J, Tops BB, Idema AJ, Rivera AL, Bleeker FE, Gijtenbeek AM, Diefes K, Heathcock L, Aldape KD, Jeuken JW, Wesseling P (2013) Significance of complete 1p/19q co-deletion, IDH1 mutation and MGMT promoter methylation in gliomas: use with caution. *Mod Pathol* 26(7):922–9
- Chamberlain MC, Born D (2015) Prognostic significance of relative 1p/19q codeletion in oligodendroglial tumors. *J Neuro Oncol* 125(2):249–251
- Louis DN, Perry A, Reifenberger G, von Deimling A, Figarella-Branger D, Cavenee WK, Ohgaki H, Wiestler OD, Kleihues P, Ellison DW (2016) The 2016 World Health Organization classification of tumors of the central nervous system: a summary. *Acta Neuropathol* 131(6):803–820
- Macarena I, Young RJ, Rubel J, Rosenblum M, Tisnado J, Briggs S, Arevalo-Perez J, Cross JR, Campos C, Straley K (2016) Integration of 2-hydroxyglutarate-proton magnetic resonance spectroscopy into clinical practice for disease monitoring in isocitrate dehydrogenase-mutant glioma. *Neuro Oncology* 18(2):283–290
- Pope WB, Prins RM, Thomas MA, Nagarajan R, Yen KE, Bittinger MA, Salamon N, Chou AP, Yong WH, Soto H (2012) Non-invasive detection of 2-hydroxyglutarate and other metabolites in IDH1 mutant glioma patients using magnetic resonance spectroscopy. *J Neuro Oncol* 107(1):197–205
- Andronesi OC, Rapalino O, Gerstner E, Chi A, Batchelor TT, Cahill DP, Sorensen AG, Rosen BR (2013) Detection of oncogenic IDH1 mutations using magnetic resonance spectroscopy of 2-hydroxyglutarate. *J Clin Invest* 123(9):3659–3663
- Lee S, Choi SH, Ryoo I, Yoon TJ, Kim TM, Lee S-H, Park C-K, Kim J-H, Sohn C-H, Park S-H (2015) Evaluation of the microenvironmental heterogeneity in high-grade gliomas with IDH1/2 gene mutation using histogram analysis of diffusion-weighted imaging and dynamic-susceptibility contrast perfusion imaging. *J Neuro Oncol* 121(1):141–150

12. Yamashita K, Hiwatashi A, Togao O, Kikuchi K, Hatae R, Yoshimoto K, Mizoguchi M, Suzuki S, Yoshiura T, Honda H (2016) MR imaging-based analysis of glioblastoma multiforme: estimation of IDH1 mutation status. *Am J Neuroradiol* 37(1):58–65
13. Yu J, Shi Z, Lian Y, Li Z, Liu T, Gao Y, Wang Y, Chen L, Mao Y (2017) Noninvasive IDH1 mutation estimation based on a quantitative radiomics approach for grade II glioma. *Eur Radiol* 27(8):3509–3522
14. Zhang B, Chang K, Ramkissoon S, Tanguturi S, Bi WL, Reardon DA, Ligon KL, Alexander BM, Wen PY, Huang RY (2017) Multimodal MRI features predict isocitrate dehydrogenase genotype in high-grade gliomas. *Neuro Oncology* 19(1):109–117
15. Yu J, Shi Z, Ji C, Lian Y, Wang Y, Chen L, Mao Y (2016) Anatomical location differences between mutated and wild-type isocitrate dehydrogenase 1 in low-grade gliomas. *Int J Neurosci* 2017:1–8
16. Akkus Z, Ali I, Sedlar J, Kline TL, Agrawal JP, Parney IF, Giannini C, Erickson BJ (2016) Predicting 1p19q chromosomal deletion of low-grade gliomas from MR images using deep learning. *arXiv preprint arXiv:1611.06939*
17. Zhou H, Vallières M, Bai HX, Su C, Tang H, Oldridge D, Zhang Z, Xiao B, Liao W, Tao Y (2017) MRI features predict survival and molecular markers in diffuse lower-grade gliomas. *Neuro Oncology* 19(6):862–870
18. Aerts HJ, Velazquez ER, Leijenaar RT, Parmar C, Grossmann P, Carvalho S, Bussink J, Monshouwer R, Haibe-Kains B, Rietveld D (2014) Decoding tumour phenotype by noninvasive imaging using a quantitative radiomics approach. *Nat Commun* 3(5):4006
19. Lambin P, Rios-Velazquez E, Leijenaar R, Carvalho S, van Stiphout RG, Granton P, Zegers CM, Gillies R, Boellard R, Dekker A (2012) Radiomics: extracting more information from medical images using advanced feature analysis. *Eur J Cancer* 48(4):441–446
20. Gillies RJ, Kinahan PE, Hricak H (2015) Radiomics: images are more than pictures, they are data. *Radiology* 278(2):563–577
21. Kotrotsou A, Zinn PO, Colen RR (2016) Radiomics in brain tumors: an emerging technique for characterization of tumor environment. *Magn Reson Imaging Clin N Am* 24(4):719–729
22. Lavon I, Refael M, Zelikovitch B, Shalom E, Siegal T (2010) Serum DNA can define tumor-specific genetic and epigenetic markers in gliomas of various grades. *Neuro Oncology* 12(2):173–180
23. Jenkinson M, Smith S (2001) A global optimisation method for robust affine registration of brain images. *Med Image Anal* 5(2):143–156
24. Smith SM (2002) Fast robust automated brain extraction. *Hum Brain Mapp* 17(3):143–155
25. Zhang Y, Brady M, Smith S (2001) Segmentation of brain MR images through a hidden Markov random field model and the expectation–maximization algorithm. *IEEE Trans Med Imaging* 20(1):45–57
26. Haralick RM, Shanmugam K (1973) Textural features for image classification. *IEEE Trans Syst Man Cybern* 6:610–621
27. Kickingereder P, Bonekamp D, Nowosielski M, Kratz A, Sill M, Burth S, Wick A, Eidel O, Schlemmer HP, Radbruch A, Debus J, Herold-Mende C, Unterberg A, Jones D, Pfister S, Wick W, von Deimling A, Bendszus M, Capper D (2016) Radiogenomics of glioblastoma: machine learning-based classification of molecular characteristics by using multiparametric and multiregional MR imaging features. *Radiology* 281(3):907–918
28. Kassner A, Thornhill RE (2010) Texture analysis: a review of neurologic MR imaging applications. *AJNR Am J Neuroradiol* 31(5):809–816
29. Skogen K, Schulz A, Dormagen JB, Ganeshan B, Helseth E, Server A (2016) Diagnostic performance of texture analysis on MRI in grading cerebral gliomas. *Eur J Radiol* 85(4):824–829
30. Chang EF, Smith JS, Chang SM, Lamborn KR, Prados MD, Butowski N, Barbaro NM, Parsa AT, Berger MS, McDermott MM (2008) Preoperative prognostic classification system for hemispheric low-grade gliomas in adults. *J Neurosurg* 109(5):817–824
31. Zlatescu MC, TehraniYazdi A, Sasaki H, Megyesi JF, Betensky RA, Louis DN, Cairncross JG (2001) Tumor location and growth pattern correlate with genetic signature in oligodendroglial neoplasms. *Cancer Res* 61(18):6713–6715